ETH
Eidgenössische Technische Hochschule Zürich
Swiss Federal Institute of Technology Zurich

Seminar for Applied Mathematics SAM

Modelling the active cochlea as a fully-coupled system of subwavelength Hopf resonators

H. Ammari and B. Davies

Research Report No. 2019-20

April 2019
Latest revision: April 2019

Seminar für Angewandte Mathematik
Eidgenössische Technische Hochschule
CH-8092 Zürich
Switzerland

Modelling the active cochlea as a fully-coupled system of subwavelength Hopf resonators

Habib Ammari* Bryn Davies*

Abstract

We combine recent breakthroughs in coupled subwavelength resonator mechanics with the theory of cochlear Hopf resonators in order to better understand the active cochlea. We model the acoustic pressure on the surface of the basilar membrane, offering an understanding of how this couples the array of hair cells. By decomposing the behaviour over the system's resonant modes, we are able to offer explanations for several of the inner ear's key properties, including its frequency selectivity, nonlinear amplification and two-tone response.

Mathematics subject classification: 35C20, 35Q92
Keywords: subwavelength resonance, coupled Hopf resonators, active cochlear mechanics, hybridisation, nonlinear cochlear amplifier, two-tone interference

1 Introduction

In the 1850s, Hermann von Helmholtz proposed a cochlear model based on an array of resonators tuned to different audible frequencies distributed along the length of the cochlea [17]. More recently, bundles of cylindrical cells known as hair cells have been identified as candidate resonant elements [6]. These cells are 20-70µm tall and are distributed along the basilar membrane increasing in size from base to apex [26, 12].

Following developments made in the second half of the 20$^{\text{th}}$ century, it is now known that the cochlea employs an active response mechanism in its function, thanks to motor proteins within its hair cells (a process known as somatic motility) [20, 23]. Indeed, some of the cochlea's most remarkable abilities could not be produced by a passive system. There is evidence that this active mechanism acts via a positive feedback loop, giving a nonlinear amplification effect, however understanding the precise details of this system represents one of the most fundamental open questions in understanding auditory perception [16, 25].

*Department of Mathematics, ETH Zrich, Rmistrasse 101, CH-8092 Zrich, Switzerland (habib.ammari@sam.math.ethz.ch, bryn.davies@sam.math.ethz.ch).

1.1 Hopf resonators in cochlear mechanics

Hopf resonators have become popular objects to study thanks to their remarkable ability to account for the key properties that typify cochlear behaviour [18, 19, 14, 20, 13, 23]. The normal form of a single Hopf resonator $z = z(t) : \mathbb{R} \to \mathbb{C}$ in the complex plane is given by the forced differential equation

$$\frac{\mathrm{d}z}{\mathrm{d}t} = (\mu + i\omega_0)z - |z|^2 z + F, \tag{1}$$

where $F = F(t)$ is the forcing term and ω_0 and μ are real parameters. This system is a resonator in the sense that the absolute value of the response z is greatest when the forcing F occurs with frequency ω_0.

The parameter μ is the bifurcation parameter. For $\mu < 0$ the unforced system ($F = 0$) has a stable equilibrium at $z = 0$ whereas when $\mu > 0$ this equilibrium is unstable and there exists a stable limit cycle $z(t) = \sqrt{\mu}e^{i\omega_0 t}$. This birth of a limit cycle is characteristic of a (supercritical) Hopf bifurcation. For further details see *e.g.* [33].

The cochlea demonstrates exceptionally good frequency selectivity. Even individuals without musical training can detect tones differing in frequency by less than 0.5% [18, 11]. The excitation of system (1) at frequencies close to ω_0 is able to account for this frequency selectivity.

The cochlea is able to detect sounds with amplitudes ranging over six orders of magnitude [19, 21]. This relies on an ability to amplify sounds according to a compressive nonlinearity whereby quiet sounds are amplified much more greatly than louder ones [29]. This property is produced by the cubic term in (1). Further, the one-third power law ($|z| \sim |F|^{1/3}$) associated with the solution of (1) close to bifurcation (when μ is small) matches quantitatively with the responsiveness observed in the cochlea [18, 21].

A further symptom of the nonlinearity that exists in the cochlea is the behaviour that is observed under the influence of a signal composed of two distinct tones. It is firstly seen that when the ear is excited by such a stimulus two-tone suppression occurs. That is, the frequency spectrum of the response contains the expected two amplitude peaks, however, these are smaller than each would be in the absence of the other tone [30]. Further, it has been known since the 18^{th} century that in such a situation the ear also detects additional tones, variously known as combination tones, distortion products or Tartini's tones after the Italian violinist Giuseppe Tartini [17, 28, 21]. Close to bifurcation, the nonlinearity in (1) gives products that can account for these phenomena [21, 13].

In this work, we will combine the capabilities of Hopf resonators with recent breakthroughs in understanding the acoustic coupling that occurs between hair cells [1]. We will study the acoustic pressure on the (two-dimensional) surface of the basilar membrane and will explore a model based on the standard wave equation for the propagation of sound waves, but with the addition of a "$|z|^2 z$"-inspired forcing term. A thorough discussion of the evidence supporting the

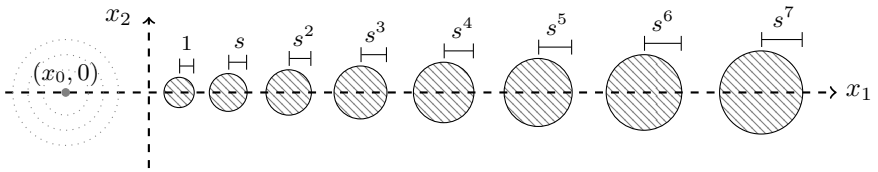

Figure 1: An array of eight (circular) subdomains $D = D_1 \cup \cdots \cup D_8$, graded in size with factor $s > 1$ and arranged linearly along $x_2 = 0$. The separation between bubbles is assumed to grow in proportion to the size. The point source is shown at $(x_0, 0) \in \mathbb{R}^2$ on the negative x_1-axis.

modelling of hair cells as compressible elements that are excited by a pressure wave in the cochlea is given in [5, 7], while the implications of such a model are explored in [1]. We will show that when subjected to Hopf-type amplification and coupled by variations in acoustic pressure, a simple model of a linear array of hair cells can describe many of the above behaviours.

1.2 Problem formulation

Consider a domain D in $\mathbb{R}^2$ which is the disjoint union of $N \in \mathbb{N}$ bounded and simply connected subdomains $\{D_1, \ldots, D_N\}$. Each subdomain ∂D_n represents a hair cell bundle and is assumed to be such that there exists some $0 < \alpha < 1$ so that $\partial D_n \in C^{1,\alpha}$ (that is, each ∂D_n is locally the graph of a differentiable function whose derivatives are Hölder continuous with exponent α).

We consider an acoustic pressure wave that is emitted by a point source and scattered by D. The point source will be located at a point $(x_0, 0) \in \mathbb{R}^2$ on the negative x_1-axis, so as to represent the signal entering the base of the cochlea. We will consider the bundles arranged in a straight line since the curvature of the cochlea does not contribute to its mechanical behaviour [12]. Figure 1 shows an example of such an arrangement, where $x = (x_1, x_2) \in \mathbb{R}^2$ represents the position on the surface of the basilar membrane.

We consider the effect of a nonlinear forcing term $\partial_t p |\partial_t p|^2$, inspired by the discussion in Section 1.1. The incoming signal is represented by a forcing term $f(t)$ at $(x_0, 0)$. We denote by ρ_b and κ_b the density and bulk modulus of the interior of the cell bundles, respectively, and denote by ρ and κ the corresponding parameters for the auditory fluid (which we assume occupies $\mathbb{R}^2 \setminus \overline{D}$). We may then denote the acoustic wave speeds in $\mathbb{R}^2 \setminus \overline{D}$ and in D respectively by

$$v = \sqrt{\frac{\kappa}{\rho}}, \quad v_b = \sqrt{\frac{\kappa_b}{\rho_b}}. \tag{2}$$

The propagation of the acoustic pressure wave $p = p(x, t)$ is then given by the problem

$$\begin{cases} \left(\Delta - \frac{1}{v^2}\frac{\partial^2}{\partial t^2}\right) p = \frac{1}{v^2} f(t)\delta_{(x_0,0)}(x), & \text{for } (x,t) \in \mathbb{R}^2 \setminus \overline{D} \times \mathbb{R}, \\ \left(\Delta - \frac{1}{v_b^2}\frac{\partial^2}{\partial t^2}\right) p = \frac{\beta}{v_b^2} |\frac{\partial p}{\partial t}|^2 \frac{\partial p}{\partial t}, & \text{for } (x,t) \in D \times \mathbb{R}, \\ p_+ - p_- = 0, & \text{for } (x,t) \in \partial D \times \mathbb{R}, \\ \frac{1}{\rho}\frac{\partial p}{\partial \nu_x}\big|_+ - \frac{1}{\rho_b}\frac{\partial p}{\partial \nu_x}\big|_- = 0, & \text{for } (x,t) \in \partial D \times \mathbb{R}, \end{cases} \tag{3}$$

where $\frac{\partial}{\partial \nu_x}$ denotes the outward normal derivative in x and the subscripts + and - are used to denote evaluation from outside and inside ∂D respectively. $\beta \in \mathbb{R}$ is a constant that controls the magnitude of the amplification.

The comparison between (3) and the standard form of a Hopf resonator (1) close to bifurcation is particularly apparent when (3) is written in the form

$$\frac{\partial^2 p}{\partial t^2} = c(x)^2 \Delta p - \beta \left|\frac{\partial p}{\partial t}\right|^2 \frac{\partial p}{\partial t} \mathcal{X}_D(x) - f(t)\delta_{(x_0,0)}(x), \quad (x,t) \in \mathbb{R}^2 \times \mathbb{R}, \tag{4}$$

where $c(x) := v - (v - v_b)\mathcal{X}_D(x)$ and $\mathcal{X}_D$ is the characteristic function of the subset $D \subset \mathbb{R}^2$. Similar formulations are considered by *e.g.* [20, 13], for the case of a single (uncoupled) Hopf resonator.

We introduce the two dimensionless contrast parameters

$$\delta := \frac{\rho_b}{\rho}, \quad \tau := \frac{v_b}{v} = \sqrt{\frac{\rho \kappa_b}{\rho_b \kappa}}. \tag{5}$$

By rescaling the dimensions of the physical problem we may assume that

$$v = O(1), \quad v_b = O(1), \quad \tau = O(1). \tag{6}$$

We also assume that the rescaled dimensions are such that the subdomains $\{D_1, \ldots, D_N\}$ have widths that are $O(1)$. On the other hand, we assume that there is a large contrast between both the bulk moduli and the density values in $\mathbb{R}^2 \setminus \overline{D}$ and in D, so that

$$\delta \ll 1. \tag{7}$$

Such an assumption is explored at length in [5], relying on experimental determinations of the Poisson ratio of hair cells.

1.3 Coupling of graded resonators

In order to understand the interactions that occur between hair cell bundles we consider the behaviour of the system of graded resonators (3) when $f = 0$ and $\beta = 0$ (*i.e.* the unforced, passive problem).

We transform problem (3) into the complex frequency domain and are left with the Helmholtz problem

$$\begin{cases} \left(\Delta + \frac{\omega^2}{v^2}\right) u(x,\omega) = 0, & \text{for } (x,\omega) \in \mathbb{R}^2 \setminus \overline{D} \times \mathbb{C}, \\ \left(\Delta + \frac{\omega^2}{v_b^2}\right) u(x,\omega) = 0, & \text{for } (x,\omega) \in D \times \mathbb{C}, \\ u_+ - u_- = 0, & \text{for } (x,\omega) \in \partial D \times \mathbb{C}, \\ \delta \frac{\partial u}{\partial \nu}\big|_+ - \frac{\partial u}{\partial \nu}\big|_- = 0, & \text{for } (x,\omega) \in \partial D \times \mathbb{C}, \end{cases} \tag{8}$$

where we must also insist that $u(\cdot,\omega)$ satisfies the Sommerfeld radiation condition

$$\lim_{|x|\to\infty} |x|^{1/2}\left(\frac{\partial}{\partial|x|} - i\frac{\omega}{v}\right) u(x,\omega) = 0. \tag{9}$$

This condition is required to ensure that the solution represents outgoing waves (rather than incoming from infinity) and gives the well-posedness of (8).

In light of the fact that (8) contains the assumption that $f = 0$, we define the *resonances* and associated *eigenmodes* (or *resonant modes*) of (3) to be solutions $(\omega, u(\cdot,\omega)) \in \mathbb{C} \times H^1_{loc}(\mathbb{R}^2)$ of (8) with the Sommerfeld radiation condition (9). Here, $H^1_{loc}(\mathbb{R}^2)$ is the space of functions that, on every compact subset of $\mathbb{R}^2$, are square integrable and have a weak first derivative that is also square integrable. We are particularly interested in solutions where ω is small and the cell bundles are much smaller than the wavelength of the associated radiation (as is the case with hair cells, when compared to the wavelength of audible sound). Such solutions are known as *subwavelength* modes.

In [1] it is shown that the system of N coupled resonators $D = D_1 \cup \cdots \cup D_N$ has N subwavelength resonances $\omega_1, \ldots, \omega_N$ and associated eigenmodes $u_1(x), \ldots, u_N(x)$. The argument is based on representing the solution $u(x,\omega)$ to (8) as

$$u(x,\omega) = \begin{cases} \mathcal{S}_D^{\omega/v}[\psi](x), & (x,\omega) \in \mathbb{R}^2 \setminus \overline{D} \times \mathbb{C}, \\ \mathcal{S}_D^{\omega/v_b}[\phi](x), & (x,\omega) \in D \times \mathbb{C}, \end{cases} \tag{10}$$

for some surface potentials $\phi, \psi \in L^2(\partial D)$ where $\mathcal{S}_D$ is the *Helmholtz single layer potential* associated with the domain D. This integral operator is defined as

$$\mathcal{S}_D^k[\varphi](x) := \int_{\partial D} \Gamma^k(x-y)\varphi(y)\, d\sigma(y), \quad x \in \partial D, \varphi \in L^2(\partial D), k \in \mathbb{C}, \tag{11}$$

where Γ^k is the outgoing (*i.e.* satisfying the Sommerfeld radiation condition) fundamental solution to the Helmholtz operator $\Delta + k^2$ in $\mathbb{R}^2$ [2].

A detailed examination of the resonances and eigenmodes can be found in [1]. The crucial result is that, when the incoming signal has a wavelength that is much larger than the physical dimensions of the resonators, the behaviour of the system can be approximated by decomposing the solution over the space spanned by the subwavelength eigenmodes. In the case of audible sound (whose wavelength in cochlear fluid ranges from a few centimetres to several metres) being scattered by hair cells measuring tens of micrometres, this approximation gives a comprehensive description of the system's behaviour.

In order to improve computational efficiency, we assume in this work that the cell bundles are circular. This means that we can use the multipole expansion method, an explanation of which is provided in *e.g.* [3, Appendix C]. The method relies on the idea that functions in $L^2(\partial D)$ are, on each *circular* ∂D_i, 2π-periodic so we may approximate by the leading order terms of a Fourier series representation.

2 Coupled Hopf system

We decompose the motion of system (3) into the N subwavelength resonant modes by writing

$$p(x,t) \simeq \mathrm{Re}\left(\sum_{n=1}^{N} \alpha_n(t) u_n(x)\right), \tag{12}$$

for some complex-valued functions of time $\alpha_1(t), \ldots, \alpha_N(t)$.

In light of the transmission properties (across ∂D) that the eigenmodes inherit from (8), we reach the problem

$$\begin{aligned} \sum_{n=1}^{N} \big(\alpha_n''(t) + \omega_n^2 \alpha_n(t)\big) u_n(x) + f(t)\delta_{(x_0,0)}(x) \\ + \beta \left(\sum_{n=1}^{N} \alpha_n'(t) u_n(x)\right)^2 \left(\sum_{n=1}^{N} \overline{\alpha_n'(t)}\,\overline{u_n(x)}\right) \mathcal{X}_D(x) = 0. \end{aligned} \tag{13}$$

We now fix some large domain Q in $\mathbb{R}^2$ that contains all the resonators as well as the point source (*i.e.* $D \cup \{(x_0,0)\} \subset Q$). Then we may define $\gamma \in \mathbb{C}^{N\times N}$ to be the square matrix with entries

$$\gamma_{i,j} := \int_Q u_i(x)\overline{u_j(x)}\,dx = (u_i, u_j)_Q, \tag{14}$$

for $i,j = 1,\ldots,N$. As a consequence of the linear independence of the eigenmodes, γ is invertible [1].

We are then in a position to take the $L^2(Q)$ product of (13) with u_m for $m = 1,\ldots,N$, reaching a system of N equations in t given by

$$\gamma^T \begin{pmatrix} \alpha_1'' + \omega_1^2\alpha_1 \\ \vdots \\ \alpha_N'' + \omega_N^2\alpha_N \end{pmatrix} + f \begin{pmatrix} (\delta_{(x_0,0)}, u_1)_Q \\ \vdots \\ (\delta_{(x_0,0)}, u_N)_Q \end{pmatrix} + \beta \begin{pmatrix} ((\sum \alpha_n' u_n)^2 \sum \overline{\alpha_n' u_n}, u_1)_D \\ \vdots \\ ((\sum \alpha_n' u_n)^2 \sum \overline{\alpha_n' u_n}, u_N)_D \end{pmatrix} = 0. \tag{15}$$

2.1 Pure-tone response

Consider the case of an incoming signal that consists of a single pure tone at frequency Ω, that is, $f(t) = \mathrm{Re}(Fe^{i\Omega t})$ for $F, \Omega \in \mathbb{R}$. In this case, we may represent the solutions to (15) as $\alpha_n(t) = X_n e^{i\Omega t}$ for complex amplitudes $X_n \in \mathbb{C}$ [20, 33, 15]. This gives the coupled equations for $m = 1,\ldots,N$

$$\begin{aligned} (\omega_m^2 - \Omega^2) X_m + F \sum_{n=1}^{N} [\gamma^{-1}]_{n,m} (\delta_{(x_0,0)}, u_n)_Q \\ - i\Omega^3 \beta \sum_{n=1}^{N} [\gamma^{-1}]_{n,m} \left(\sum_{i,j,k=1}^{N} X_i X_j \overline{X_k} (u_i u_j \overline{u_k}, u_n)_D\right) = 0. \end{aligned} \tag{16}$$

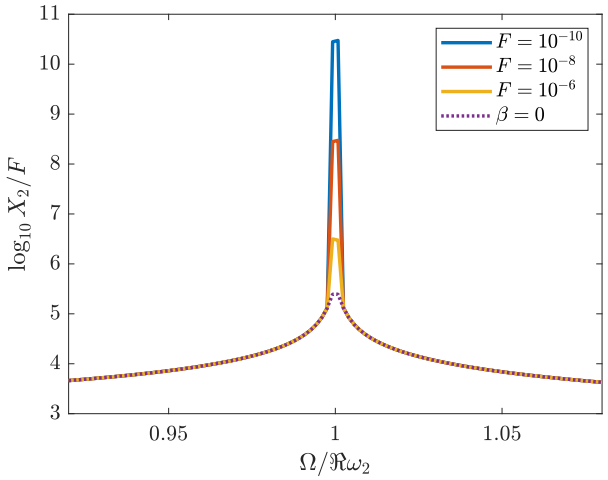

Figure 2: Nonlinear amplification in the coupled Hopf system at resonance. We show how the response X_2/F varies with incoming frequency Ω in system (16) for difference forcing magnitudes F. The response of the second eigenmode in a system of $N = 6$ cell bundles is studied. The dashed line shows the case where the cubic nonlinearity has been removed (giving a passive system) for comparison.

The results of solving (16) numerically for $X_1, \ldots, X_N$ are shown in Figure 2. There is a sharply increased response when Ω is close to the resonant frequency associated with the eigenmode. Different magnitudes of force F are shown. When the force is smaller, the response is much greater, thereby allowing the model to capture a very large range of forcing amplitudes with only relatively small variations in acoustic pressure. The sharper response of the active system will also improve frequency resolution, compared to the passive model.

In Figure 3 we study how the oscillations of the solution to Equation (16) lag behind the forcing, as is common in a coupled system of forced oscillators. This is achieved by writing the solution (12) as

$$p(x,t) \simeq \mathrm{Re}\left(\sum_{n=1}^{N} X_n e^{i\Omega t} u_n(x)\right) = \mathrm{Re}\left(R(x)e^{i(\Omega t+\phi(x))}\right), \tag{17}$$

for real constants R and ϕ, the latter of which represents the phase delay. ϕ in (17) is, in principle, defined such that $0 \leq \phi < 2\pi$, however the assumption that ϕ should be a continuous function of Ω leads to the phase delays of multiple cycles seen in Figure 3. The group delay, the time required for information to be delivered, is then given by the quantity $\mathrm{d}\phi/\mathrm{d}\Omega$ [10].

The behaviour in Figure 3 shows many similarities to experimental observations [29, 32]. In Figure 3 (Left), it is notable that the curves all start at a phase delay of approximately minus a quarter cycle and the delay then increases with increasing frequency. There is a tendency for curves to group around values

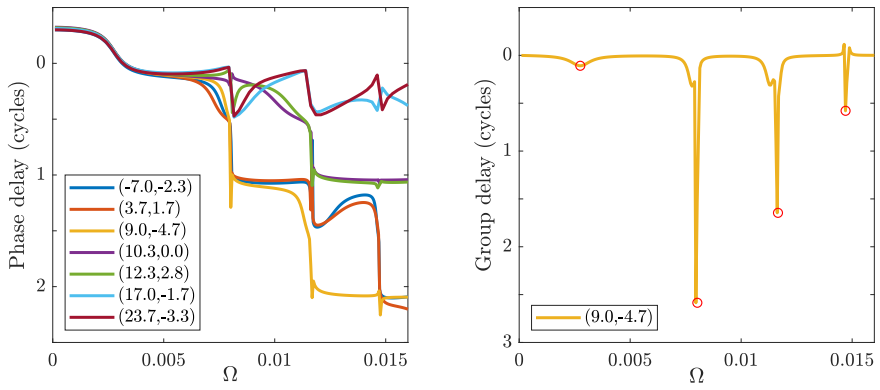

Figure 3: The phase and group delays of the response of the coupled Hopf system. Left: We show how the phase delay (in cycles) varies as a function of the incoming frequency Ω at different points $x = (x_1, x_2)$ on the basilar membrane. Right: We show, for just one of the points, how the group delay (in cycles) varies as a function of Ω. The circles denote the position of resonant frequencies of the system ($\Omega = \operatorname{Re}\omega_1, \operatorname{Re}\omega_2, \operatorname{Re}\omega_3, \operatorname{Re}\omega_4$, respectively). In both cases, a system of $N = 6$ cells arranged along the line $x_2 = 0$ is studied.

separated by a full cycle. Known as "phase plateaus", this behaviour has been widely observed by experimentalists [27].

In Figure 3 (Right), it is seen that in the region of one of the system's resonant frequencies the group delay can reach several cycles. These values are typical of the cochlea and represent an important consideration when evaluating a Helmholtz-inspired, resonance-based model [6].

2.2 Two-tone interference

Consider the case of an incoming signal composed of two pure tones. We explore the response to such a stimulus by considering forcing of the form

$$f(t) = \operatorname{Re}\left(F_1 e^{i\Omega_1 t} + F_2 e^{i\Omega_2 t}\right), \tag{18}$$

in system (15). In this case the response, captured by the complex-valued functions $\alpha_1(t), \ldots, \alpha_N(t)$, will contain contributions from all the Fourier amplitudes with frequencies $p\Omega_1 + q\Omega_2$ for integers $p, q \in \mathbb{Z}$ [21]. Thus, for each $n = 1, \ldots, N$ there exist $X_{p,q}^{(n)} \in \mathbb{C}$, $p, q \in \mathbb{Z}$ such that

$$\alpha_n(t) = \sum_{p,q=-\infty}^{\infty} X_{p,q}^{(n)} e^{i(p\Omega_1 + q\Omega_2)t}. \tag{19}$$

The expansion (19) is dominated by the terms with small $|p|+|q|$ [21, 24, 31]. As a result, it makes sense to refer to $|p|+|q|$ as the *order* of $X_{p,q}$. In particular, it is found in [31] that the amplitudes approximately obey the law $X_{p,q} \sim X_{1,0}^{|p|} X_{0,1}^{|q|}$ and thus diminish with increasing order (for small amplitudes).

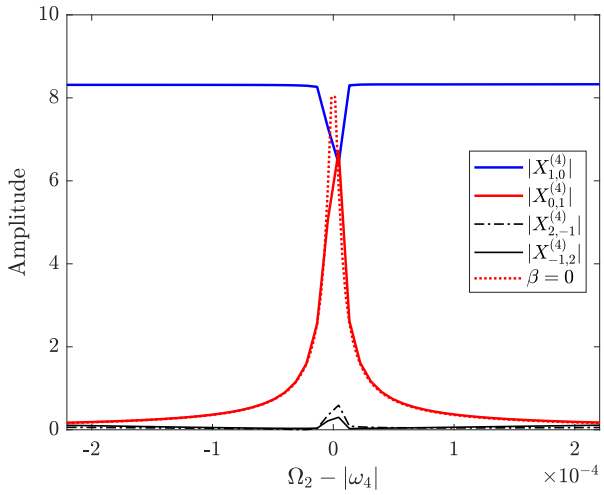

Figure 4: Two-tone interference in the coupled Hopf system. We study the fourth eigenmode in a system of $N = 6$ cells and show how the absolute values of the leading order coefficients vary in the case that $\Omega_1 = |\omega_4|$ is fixed and Ω_2 is varied. We use $F_1 = F_2 = 10^{-5}$. The red dashed line shows $X^{(4)}_{0,1}$ in the case where the cubic nonlinearity has been removed (giving a passive system) for comparison.

We substitute the expansion (19) into (15). The effect of the cubic nonlinearity is that many terms, including all those of even order, must vanish. We find that, for small amplitudes, we can approximate (19) by

$$\begin{aligned}\alpha_n(t) \simeq X^{(n)}_{1,0} e^{i\Omega_1 t} + X^{(n)}_{0,1} e^{i\Omega_2 t} \\ + X^{(n)}_{2,-1} e^{i(2\Omega_1 - \Omega_2)t} + X^{(n)}_{-1,2} e^{i(-\Omega_1 + 2\Omega_2)t}.\end{aligned} \tag{20}$$

By comparing the coefficients of the dominant modes $e^{i\Omega_1 t}$, $e^{i\Omega_2 t}$, $e^{i(2\Omega_1 - \Omega_2)t}$ and $e^{i(-\Omega_1 + 2\Omega_2)t}$ we reach a coupled system of equations that we can solve to find $\left\{ X^{(n)}_{1,0}, X^{(n)}_{0,1}, X^{(n)}_{2,-1}, X^{(n)}_{-1,2} : n = 1, \ldots, N \right\}$ (for details, see Appendix A).

Figure 4 shows the amplitudes of the four dominant Fourier modes when $\Omega_1 = |\omega_4|$ is fixed and Ω_2 is varied (in the neighbourhood of $|\omega_4|$). When Ω_2 is away from $|\omega_4|$ there appears to be little interaction between the two frequency modes. As Ω_1 and Ω_2 become close, however, two phenomena emerge. Firstly, two-tone suppression occurs. This is witnessed both by the fact that the value of $X^{(4)}_{1,0}$ drops (from its otherwise approximately constant value) and that the response of $X^{(4)}_{0,1}$ at resonance is diminished relative to the passive system. On top of this, so-called combination tones appear in the regime where Ω_1 and Ω_2 are close together. These tones have frequencies $2\Omega_1 - \Omega_2$ and $-\Omega_1 + 2\Omega_2$ and occur with much smaller amplitudes than the two primary modes, as is the case when this phenomenon is observed in practice [28, 17].

3 Discussion

We have studied the acoustic pressure on the surface of the basilar membrane by combining an understanding of the coupling between an array of subwavelength resonators with the theory of Hopf resonators in cochlear mechanics. This approach has proved successful in describing several phenomena commonly exhibited by the cochlea. Firstly, it was shown in Section 2.1 that the model produced the desired frequency selectivity and nonlinear amplification. The phase and group delays also showed similarities to experimental observations, particularly by taking values greater than a cycle. Then, in Section 2.2 it was further shown that the two-tone response of this coupled Hopf system both suffers from two-tone suppression and produces combination tones.

It should be emphasised that these observations have been made by studying the acoustic pressure locally on the two-dimensional surface of the basilar membrane without any consideration for the movement of the membrane itself. It was shown similarly in [1] that such a model can further account for the cochlea's tonotopic frequency map and travelling pressure wave. These conclusions suggest that coupling by acoustic pressure is an important factor in understanding cochlear mechanics and should not be disregarded.

It has been known since their first observation by David Kemp in 1978 that the ear emits sounds known as otoacoustic emissions as part of its activity [22, 34]. The ear even emits *spontaneous* otoacoustic emissions in the absence of external stimulation. This phenomenon was one of the earlier pieces of evidence supporting the active nature of the cochlea and is the most significant aspect of cochlear behaviour not accounted for by the model considered here [18]. Recent work [9, 13] has shown that a Hopf resonator can account for the production of spontaneous otoacoustic emissions by the addition of a "self-tuning" feedback loop. In our setting, this entails introducing a $\mu\partial_t p$ term to (3) and varying the parameter μ in the neighbourhood of the bifurcation. The spontaneous sounds are created when the system strays into the regime where a stable limit cycle exists.

Contrary to the linear array used in this work, hair cells in the cochlea of a mammal are arranged as one row of inner hair cells and three rows of outer hair cells. It is believed that the outer hair cells are responsible for amplification while inner hair cells act as receivers [9, 11]. In recent work, the geometric arrangement of the hair cells has been studied in an attempt to capture the cochlea's behaviour [8, 4]. Using our layer potential formulation, the geometry can be easily modified providing an avenue for developing such theories.

Even with the use of the multipole method (reliant on the assumption that the cell bundles are circular) the computations in this work become expensive for large numbers of cells. In order to efficiently and concisely demonstrate the behaviour of the coupled Hopf system, the results displayed here use only small values of N. While it is feasible to study up to a few hundred cells with our current methodology, numerical computations on a model resembling a genuine mammalian cochlea (and its approximately 15,000 hair cells) are beyond the scope of our current setup. A rigorous approach to approximating the coupling

between an array of subwavelength resonators would thus represent a valuable breakthrough.

Acknowledgement

The authors would like to thank Andrew Bell for insightful comments made on an early version of this manuscript.

A Appendix: Two-tone interference

By writing the amplitudes $\alpha_n(t)$ in the approximate form given in (20) we are able to rewrite the decomposition of $p(x,t)$ in (12) in terms of the dominant Fourier amplitudes

$$\begin{aligned} p(x,t) = &\left(\sum_{n=1}^{N} X_{1,0}^{(n)} u_n(x)\right) e^{i\Omega_1 t} + \left(\sum_{n=1}^{N} X_{0,1}^{(n)} u_n(x)\right) e^{i\Omega_2 t} \\ &+ \left(\sum_{n=1}^{N} X_{2,-1}^{(n)} u_n(x)\right) e^{i(2\Omega_1-\Omega_2)t} + \left(\sum_{n=1}^{N} X_{-1,2}^{(n)} u_n(x)\right) e^{i(-\Omega_1+2\Omega_2)t}, \end{aligned} \tag{21}$$

from which we see that it is convenient to define the sums

$$\begin{aligned} S_{1,0}(x) &:= \Omega_1 \sum_{n=1}^{N} X_{1,0}^{(n)} u_n(x), \quad S_{0,1}(x) := \Omega_2 \sum_{n=1}^{N} X_{0,1}^{(n)} u_n(x), \\ S_{2,-1}(x) &:= (2\Omega_1 - \Omega_2) \sum_{n=1}^{N} X_{2,-1}^{(n)} u_n(x), \\ S_{-1,2}(x) &:= (-\Omega_1 + 2\Omega_2) \sum_{n=1}^{N} X_{-1,2}^{(n)} u_n(x). \end{aligned}$$

We then wish to compute the coefficients of the Fourier modes $e^{i\Omega_1 t}$, $e^{i\Omega_2 t}$, $e^{i(2\Omega_1-\Omega_2)t}$ and $e^{i(-\Omega_1+2\Omega_2)t}$ when we substitute (21) into the cubic nonlinearity $|\partial_t p|^2 \partial_t p$. We find that these coefficients are respectively given by

$$\begin{aligned} C_{1,0} &:= S_{1,0}|S_{1,0}|^2 + 2S_{1,0}\big[|S_{0,1}|^2 + |S_{2,-1}|^2 + |S_{-1,2}|^2\big] \\ &\qquad + S_{0,1}^2\overline{S_{-1,2}} + 2S_{0,1}S_{2,-1}\overline{S_{1,0}} + 2S_{2,-1}S_{-1,2}\overline{S_{0,1}}, \\ C_{0,1} &:= S_{0,1}|S_{0,1}|^2 + 2S_{0,1}\big[|S_{1,0}|^2 + |S_{2,-1}|^2 + |S_{-1,2}|^2\big] \\ &\qquad + S_{1,0}^2\overline{S_{2,-1}} + 2S_{1,0}S_{-1,2}\overline{S_{0,1}} + 2S_{2,-1}S_{-1,2}\overline{S_{1,0}}, \\ C_{2,-1} &:= S_{2,-1}|S_{2,-1}|^2 + 2S_{2,-1}\big[|S_{1,0}|^2 + |S_{0,1}|^2 + |S_{-1,2}|^2\big] \\ &\qquad + S_{1,0}^2\overline{S_{0,1}} + 2S_{1,0}S_{0,1}\overline{S_{-1,2}}, \end{aligned}$$

$$C_{-1,2} := S_{-1,2}|S_{-1,2}|^2 + 2S_{-1,2}\big[|S_{1,0}|^2 + |S_{0,1}|^2 + |S_{2,-1}|^2\big] + S_{0,1}^2\overline{S_{1,0}} + 2S_{1,0}S_{0,1}\overline{S_{2,-1}}.$$

It is then more straightforward to see that when we substitute (20) into system (15) and equate coefficients of the Fourier modes $e^{i\Omega_1 t}$, $e^{i\Omega_2 t}$, $e^{i(2\Omega_1-\Omega_2)t}$ and $e^{i(-\Omega_1+2\Omega_2)t}$ we reach the four coupled systems given by

$$\gamma^T \begin{pmatrix} (\omega_1^2-\Omega_1^2)X_{1,0}^{(1)} \\ \vdots \\ (\omega_N^2-\Omega_1^2)X_{1,0}^{(N)} \end{pmatrix} + F_1 \begin{pmatrix} (\delta_{(x_0,0)},u_1)_Q \\ \vdots \\ (\delta_{(x_0,0)},u_N)_Q \end{pmatrix} - i\beta \begin{pmatrix} (C_{1,0},u_1)_D \\ \vdots \\ (C_{1,0},u_N)_D \end{pmatrix} = 0, \quad (22)$$

$$\gamma^T \begin{pmatrix} (\omega_1^2-\Omega_2^2)X_{0,1}^{(1)} \\ \vdots \\ (\omega_N^2-\Omega_2^2)X_{0,1}^{(N)} \end{pmatrix} + F_2 \begin{pmatrix} (\delta_{(x_0,0)},u_1)_Q \\ \vdots \\ (\delta_{(x_0,0)},u_N)_Q \end{pmatrix} - i\beta \begin{pmatrix} (C_{0,1},u_1)_D \\ \vdots \\ (C_{0,1},u_N)_D \end{pmatrix} = 0, \quad (23)$$

$$\gamma^T \begin{pmatrix} (\omega_1^2-(2\Omega_1-\Omega_2)^2)X_{2,-1}^{(1)} \\ \vdots \\ (\omega_N^2-(2\Omega_1-\Omega_2)^2)X_{2,-1}^{(N)} \end{pmatrix} - i\beta \begin{pmatrix} (C_{2,-1},u_1)_D \\ \vdots \\ (C_{2,-1},u_N)_D \end{pmatrix} = 0, \quad (24)$$

$$\gamma^T \begin{pmatrix} (\omega_1^2-(-\Omega_1+2\Omega_2)^2)X_{-1,2}^{(1)} \\ \vdots \\ (\omega_N^2-(-\Omega_1+2\Omega_2)^2)X_{-1,2}^{(N)} \end{pmatrix} - i\beta \begin{pmatrix} (C_{-1,2},u_1)_D \\ \vdots \\ (C_{-1,2},u_N)_D \end{pmatrix} = 0, \quad (25)$$

which we can solve numerically to find $\Big\{X_{1,0}^{(n)}, X_{0,1}^{(n)}, X_{2,-1}^{(n)}, X_{-1,2}^{(n)} : n = 1,\dots,N\Big\}$.

References

[1] Ammari, H. and Davies, B. (2019). A fully-coupled subwavelength resonance approach to modelling the passive cochlea. *arXiv preprint arXiv:1901.08808*.

[2] Ammari, H., Fitzpatrick, B., Kang, H., Ruiz, M., Yu, S., and Zhang, H. (2018). *Mathematical and computational methods in photonics and phononics*, volume 235 of *Mathematical Surveys and Monographs*. American Mathematical Society, Providence.

[3] Ammari, H., Fitzpatrick, B., Lee, H., Yu, S., and Zhang, H. (2017). Subwavelength phononic bandgap opening in bubbly media. *J. Differ. Equations*, 263(9):5610–5629.

[4] Bell, A. (2002). Musical ratios in geometrical spacing of outer hair cells in the cochlea: strings of an underwater piano? In Stevens, C., Burnham, D., McPherson, G., Schubert, E., and Renwick, J., editors, *Proceedings of the 7th international conference on music perception and cognition*, Sydney. Causal Productions, Adelaide.

[5] Bell, A. (2005). *The underwater piano: a resonance theory of cochlear mechanics*. PhD thesis, The Australian National University.

[6] Bell, A. (2012). A resonance approach to cochlear mechanics. *P. L. o. S. One*, 7(11):e47918.

[7] Bell, A. (2018). New perspectives on old ideas in hearing science: intralabyrinthine pressure, tenotomy, and resonance. *J. Hear. Sci.*, 8(4):19–25.

[8] Bell, A. and Fletcher, N. H. (2004). The cochlear amplifier as a standing wave:squirting waves between rows of outer hair cells? *J. Acoust. Soc. Am.*, 116(2):1016–1024.

[9] Camalet, S., Duke, T., Jülicher, F., and Prost, J. (2000). Auditory sensitivity provided by self-tuned critical oscillations of hair cells. *P. Natl. Acad. Sci. U.S.A.*, 97(7):3183–3188.

[10] Claerbout, J. F. (1992). *Earth Soundings Analysis: Processing versus Inversion*, volume 6. Blackwell Scientific Publications, London.

[11] Dallos, P. (1992). The active cochlea. *J. Neurosci.*, 12(12):4575–4585.

[12] Duifhuis, H. (2012). *Cochlear mechanics: introduction to a time domain analysis of the nonlinear cochlea*. Springer Science & Business Media, New York.

[13] Duke, T. and Jülicher, F. (2008). Critical oscillators as active elements in hearing. In *Active Processes and Otoacoustic Emissions in Hearing*, pages 63–92. Springer, New York.

[14] Eguíluz, V. M., Ospeck, M., Choe, Y., Hudspeth, A., and Magnasco, M. O. (2000). Essential nonlinearities in hearing. *Phys. Rev. Lett.*, 84(22):5232.

[15] Fletcher, N. H. (1992). *Acoustic systems in biology*. Oxford University Press, New York.

[16] Gold, T. (1948). Hearing. ii. the physical basis of the action of the cochlea. *P. Roy. Soc. Lond. B Bio.*, 135(881):492–498.

[17] Helmholtz, H. L. F. v. (1875). *On the sensations of tone as a physiological basis for the theory of music*. Longmans, Green, London.

[18] Hudspeth, A. (2008). Making an effort to listen: mechanical amplification in the ear. *Neuron*, 59(4):530–545.

[19] Hudspeth, A., Jülicher, F., and Martin, P. (2010). A critique of the critical cochlea: Hopfa bifurcationis better than none. *J. Neurophysiol.*, 104(3):1219–1229.

[20] Joyce, B. S. and Tarazaga, P. A. (2017). A study of active artificial hair cell models inspired by outer hair cell somatic motility. *J. Intel. Mat. Syst. Str.*, 28(6):811–823.

[21] Jülicher, F., Andor, D., and Duke, T. (2001). Physical basis of two-tone interference in hearing. *P. Natl. Acad. Sci. U.S.A.*, 98(16):9080–9085.

[22] Kemp, D. T. (2002). Otoacoustic emissions, their origin in cochlear function, and use. *Brit. Med. Bull.*, 63(1):223–241.

[23] Kern, A. and Stoop, R. (2003). Essential role of couplings between hearing nonlinearities. *Phys. Rev. Lett.*, 91(12):128101.

[24] Montgomery, K. (2008). Multifrequency forcing of a Hopf oscillator model of the inner ear. *Biophys. J.*, 95(3):1075–1079.

[25] Neely, S. T. and Kim, D. (1986). A model for active elements in cochlear biomechanics. *J. Acoust. Soc. Am.*, 79(5):1472–1480.

[26] Pujol, R., Lenoir, M., Ladrech, S., Tribillac, F., and Rebillard, G. (1992). Correlation between the length of outer hair cells and the frequency coding of the cochlea. In *Auditory physiology and perception*, pages 45–52. Pergammon, Oxford.

[27] Robles, L. and Ruggero, M. A. (2001). Mechanics of the mammalian cochlea. *Physiol. Rev.*, 81(3):1305–1352.

[28] Robles, L., Ruggero, M. A., and Rich, N. C. (1997). Two-tone distortion on the basilar membrane of the chinchilla cochlea. *J. Neurophysiol.*, 77(5):2385–2399.

[29] Ruggero, M. A., Rich, N. C., Recio, A., Narayan, S. S., and Robles, L. (1997). Basilar-membrane responses to tones at the base of the chinchilla cochlea. *J. Acoust. Soc. Am.*, 101(4):2151–2163.

[30] Ruggero, M. A., Robles, L., Rich, N. C., et al. (1992). Two-tone suppression in the basilar membrane of the cochlea: Mechanical basis of auditory-nerve rate suppression. *J. Neurophysiol.*, 68:1087–1087.

[31] Stoop, R., Steeb, W.-H., Gallas, J. C., and Kern, A. (2005). Auditory two-tone suppression from a subcritical Hopf cochlea. *Physica A*, 351(1):175–183.

[32] Wilson, J. P. and Evans, E. F. (1983). Some observations on the passive mechanics of cat basilar membrane. In Webster, W. R. and Aitkin, L. M., editors, *Mechanisms of Hearing*, pages 30–35. Monash University Press, Clayton, Victoria, Australia.

[33] Wong, C. W. (2013). *Introduction to mathematical physics: methods & concepts*. Oxford University Press, Oxford.

[34] Zurek, P. (1985). Acoustic emissions from the ear: A summary of results from humans and animals. *J. Acoust. Soc. Am.*, 78(1):340–344.